

# Crystal structure informed mesoscale deformation model for HCP $\text{Cu}_6\text{Sn}_5$ intermetallic compound

Anil Kunwar<sup>1,\*</sup>, Haoran Ma<sup>2,\*\*</sup>, Johan Hektor<sup>3</sup>

<sup>1</sup>Faculty of Mechanical Engineering, Silesian University of Technology, Konarskiego 18A, 44-100 Gliwice, Poland

<sup>2</sup> School of Microelectronics, Dalian University of Technology, 116024 Dalian, China

<sup>3</sup>Department of Materials Science and Applied Mathematics, Faculty of Technology and Society, Malmö University, 21119 Malmö, Sweden

\*Email (Corresponding Author): anil.kunwar@polsl.pl ; \*\*Email (Corresponding Author): mhr@dlut.edu.cn

**Abstract**—In the electronic packaging and energy storage sectors, the study of  $\text{Cu}_6\text{Sn}_5$  intermetallic compound (IMC) is getting more attention. At temperatures above 186 °C, this IMC exists in a hexagonal closed packed (HCP) crystalline structure. Crystal plasticity finite element simulations are performed on  $\text{Cu}_6\text{Sn}_5$  IMC by taking the information about its lattice parameters and direction dependent elastic properties. Three types of models corresponding to deformations in basal, prismatic and pyramidal modes are developed. With the same type of loading in the elastic regime and boundary conditions, the results of the computations reveal the differences in displacement magnitudes among the three model types.

**Keywords**— Hexagonal closed packed ; Anisotropy; Deformation; Crystal plasticity finite element; Intermetallic compound; Elastic regime

## I. INTRODUCTION

The use of Pb-free solders joints is getting promotion and significant research interest because of the immense benefit to environment and human health [1], [2]. For Sn-based solder joints using Cu substrates, the formation of joint is guaranteed by the growth of  $\text{Cu}_6\text{Sn}_5$  intermetallic compound (IMC) at the interface. For miniaturized (Pb-free) Sn-based solder joints, the volume fraction of the  $\text{Cu}_6\text{Sn}_5$  IMC in the overall composite joint can be proportionately significant. For an example, in context of 2.5D IC packaging, the diameters of solder balls can be considered in the values well below 10  $\mu\text{m}$ , and so during the reflow joining procedure with Cu substrate, the major portion of the liquid solder is consumed for the interfacial reaction and formation of the IMC. This suggests that the knowledge of the structure and properties of  $\text{Cu}_6\text{Sn}_5$  IMC can eventually help in the design of strong and reliable solder joints. Besides the electronic packaging sector, the  $\text{Cu}_6\text{Sn}_5$  IMC is known as a promising candidate materials for the electrode of the Lithium-ion battery [3].

$\text{Cu}_6\text{Sn}_5$  IMC can exist in two forms of crystalline structures [4]. At temperatures below 186 °C [3], it has a monoclinic crystalline structure, and is referred to as  $\eta'$ - $\text{Cu}_6\text{Sn}_5$ . However, for temperatures higher than 186 °C, it undergoes a structural transformation to have a hexagonal closed packed structure [5], [6]. The IMC with hexagonal closed packed (HCP) crystalline structure is also termed as  $\eta$ - $\text{Cu}_6\text{Sn}_5$ . During reflow soldering procedure, the Sn-based solder has to undergo melting and

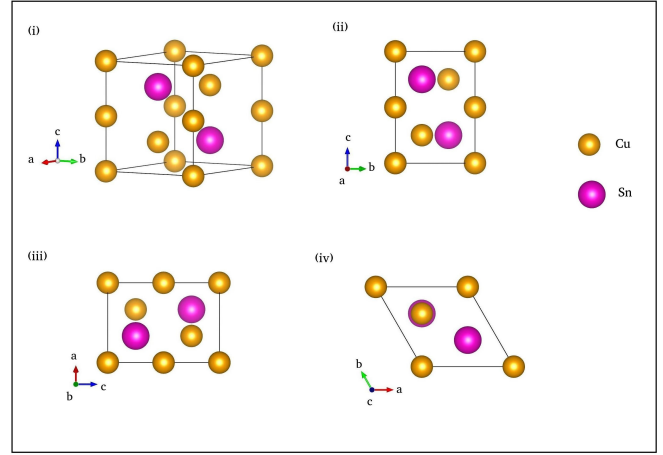


Fig. 1. Perspective view of a unit cell of  $\eta$ - $\text{Cu}_6\text{Sn}_5$  compound is presented in (i). The images in (ii), (iii) and (iv) respectively show the view along the planes normal to respectively  $\langle a \rangle$ ,  $\langle b \rangle$  and  $\langle c \rangle$  directions.

as the melting point of pure Sn is 523.15 K,  $\eta$ - $\text{Cu}_6\text{Sn}_5$  is formed during the interfacial reaction between the solder and substrate. In this study,  $\eta$ - $\text{Cu}_6\text{Sn}_5$  is considered as the material for computational analysis. The currently widespread applications such as high-powered electronic equipment and third generation semiconductor power devices have high service temperature ( $T > 523.15$  K) requirements [7], and this makes the study of  $\eta$ - $\text{Cu}_6\text{Sn}_5$  phase more relevant.

## II. COMPUTATIONAL STUDY OF THE IMC

### A. Crystal structure

The location of the the Cu atoms and Sn atoms as viewed on the unit cell of HCP  $\text{Cu}_6\text{Sn}_5$  compound is presented in Fig. 1 and that for the  $2 \times 2 \times 4$  supercell is provided in Fig. 2. The visualization is done using the Visualisation for Electronic Structural Analysis (VESTA) software [8]. The lattice parameters for the HCP crystal are  $a = b = 4.190$  Å,  $c = 5.086$  Å,  $\alpha = \beta = 90^\circ$ , and  $\gamma = 120^\circ$  [4]. The lengths  $a$ ,  $b$  and  $c$  can be the dimensions of the unit cell corresponding to  $\langle a \rangle$ ,  $\langle b \rangle$  and  $\langle c \rangle$  directions respectively. In Fig. 1(i), the

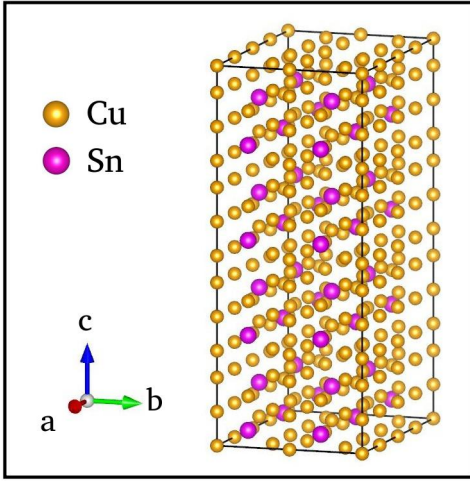


Fig. 2. The  $2 \times 2 \times 4$  supercell of the unit cell presented in Fig. 1 (i).

height of the unit cell is 5.086 Å. The views provided in Fig. 1(ii)-(iv) illustrate the angles  $\alpha$ ,  $\beta$  and  $\gamma$ .

### B. Elastic properties of $\eta$ -Cu<sub>6</sub>Sn<sub>5</sub>

The  $\eta$ -Cu<sub>6</sub>Sn<sub>5</sub>, with HCP structure, is characterized by anisotropy in elastic properties. The elasticity (stiffness) tensor ( $C_{ijkl}$ ) represents the elastic behavior of a crystalline matrix. For simplifying the models, different materials symmetry options are utilized. In this work, orthotropic symmetry is assumed for the IMC crystal. The values for the 9 components of the elasticity tensor of the IMC crystal are obtained from the work of Lee et al [9]. From the stiffness tensor, it is possible to compute and visualize direction dependent Young's moduli, Poisson's ratios and shear moduli. The images corresponding to the visualization of Young's moduli, Poisson's ratios and shear moduli are presented in Figs. 3 and 4.

The visualization of Young's moduli (Fig. 3) is done with the help of Multi-phase Elastic Aggregates (MELASA) software [10]. From the figure, it can be understood that the Young's modulus of Cu<sub>6</sub>Sn<sub>5</sub> IMC crystal is direction dependent, and its magnitude fluctuates in the range 18.15-131.75 GPa. The visualization of Poisson's ratios and shear moduli (Fig. 4) is performed using ELATE software [11]. The 3D image for variation of Poisson's ratio along the different directions is shown in Fig. 4(a). The magnitudes of the Poisson's ratio are in the range from 0.03 to 0.82. The image showing the variation of shear modulus along different direction is presented as 3D figure in Fig. 4(b) and the corresponding projections on 2D planes in Fig. 4(c). The minimum value of shear modulus is 4.8 GPa and the maximum magnitude is 51.4 GPa.

## III. CRYSTAL PLASTICITY FINITE ELEMENT SIMULATION

In context of finite strain inelastic mechanics of crystal plasticity, the deformation gradient ( $\mathbf{F}$ ) in IMC is assumed to

be composed of elastic deformation gradient ( $\mathbf{F}^e$ ) and plastic deformation gradient ( $\mathbf{F}^p$ ), as following:

$$\mathbf{F} = \mathbf{F}^e \mathbf{F}^p \quad (1)$$

where,  $\det(\mathbf{F}^e) > 0$  and  $\det(\mathbf{F}^p) = 1$ . With Cauchy stress denoted as  $\sigma$ , the following equation can be utilized to represent the Second Piola-Kirchhoff Stress:

$$\mathbf{S} = \det(\mathbf{F}) \mathbf{F}^{-1} \sigma (\mathbf{F}^{-1})^T \quad (2)$$

The HCP crystal of  $\eta$ -Cu<sub>6</sub>Sn<sub>5</sub> consists of three slip modes - (i) basal (slip system  $\{0001\} \langle 11\bar{2}0 \rangle$ ), (ii) prismatic (slip system  $\{10\bar{1}0\} \langle 11\bar{2}0 \rangle$ ); and  $\langle a \rangle$  pyramidal (slip system  $\{10\bar{1}1\} \langle 11\bar{2}0 \rangle$ ), and these modes provide deformation only to  $\langle a \rangle$  direction [12]. In addition to this, the deformation can occur via combined  $\langle c+a \rangle$  pyramidal slips (slip systems  $\{10\bar{1}1\} \langle 11\bar{2}3 \rangle$  and  $\{10\bar{2}2\} \langle 11\bar{2}3 \rangle$ ) and deformation twinning.

In this work, the deformation behavior along basal, prismatic and pyramidal modes is inspected for an IMC block. The finite element method based numerical simulations were performed in Multiphysics Object Oriented Simulation Environment (MOOSE) software [13], [14]. A cube of dimension (1 mm  $\times$  1 mm  $\times$  1 mm) is chosen as the geometry and the mesh is constructed on this geometry. A total number of 216 HEX8 mesh elements were assigned in the cube mesh. Appropriate boundaries were assigned to establish the three modes. A strain rate of  $5.0 \times 10^{-4} \text{ s}^{-1}$  was applied to one face of the cube for all of the three simulations. The elasticity tensor was supplied in the Materials block, and symmetric9 fill method is utilized to consider orthotropic symmetry of the IMC material. The information of slip systems and lattice constants (a, b and c) of the HCP crystal for Cu<sub>6</sub>Sn<sub>5</sub> IMC also was provided in the Materials block. For the current simulation, the grain size of 15  $\mu\text{m}$  is considered for the

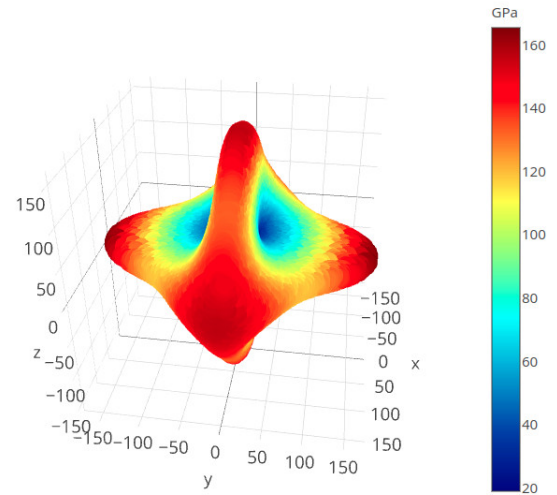


Fig. 3. Visualization of directional dependence of Young's modulus of Cu<sub>6</sub>Sn<sub>5</sub> intermetallic compound.

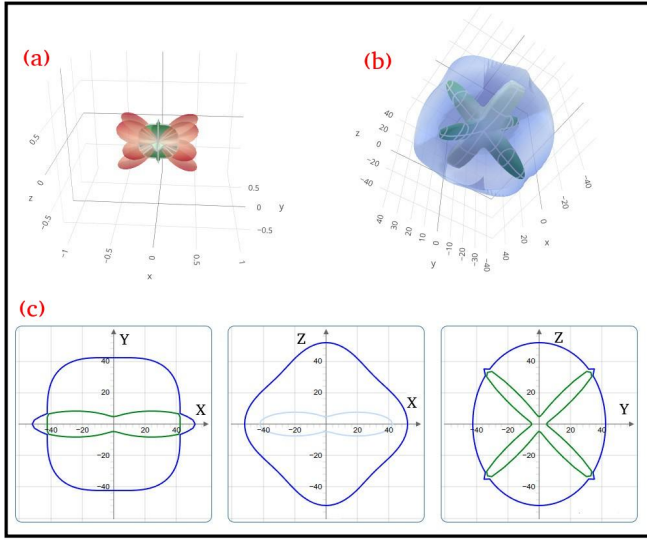


Fig. 4. Assuming the IMC as an orthotropic material, the directional dependence of poisson's ratio is illustrated in (a) whereas the spatial variation of shear modulus is presented in (b)-(c). The image in (c) corresponds to the 2D visualization of the 3D image provided in (b). The unit corresponding to the numerical values represented in (b) and (c) is GPa.

IMC grains in the cube. The temperature of the computational domain is considered to be equal to 470.0 K.

The yield strength of  $\text{Cu}_6\text{Sn}_5$  IMC is 2009 MPa [15]. Thus it should be noted that the loading described above will not be sufficient to initiate the plastic slip based deformation in the HCP crystal. Although this work will utilize the methodology of crystal plasticity finite element simulations, the following results and discussions sections will be confined within the elastic regime. That is, the stress discussed in this study will be so small that it will not induce any significant plastic deformations. The choice of elastic regime is favorable from the viewpoint of numerical convergence and computational efficiency.

#### IV. RESULTS AND DISCUSSIONS

The results for displacements at  $t=0.01$  s for simulations corresponding to basal and prismatic modes of deformation are presented in Fig. 5(a)-(b). It has to be noted that for a given strain rate, the deformation profiles for the two modes is different. The entire frontal part of the IMC cube for basal mode undergoes displacement with magnitudes larger than  $6.0\text{e-}6$  mm. Some points in the cube reach a displacement as high as  $7.6\text{e-}6$  mm. However, in case of prismatic mode, the maximum displacement reached at the top face of the cube is only  $5.24\text{E-}6$  mm. Moreover, instead of entire frontal region, the deformation is more prevalent in the top face of the cube. The displacement magnitude at  $t=0.01$  s in context of deformation corresponding to  $\langle c+a \rangle$  pyramidal mode, is presented in Fig. 6. As anticipated, for the same magnitude of applied strain rate, the cube is characterized by larger deformation at the top frontal region (as compared to two

other modes). The maximum displacement magnitude at the top regimes is around  $1.3\text{E-}5$  mm .

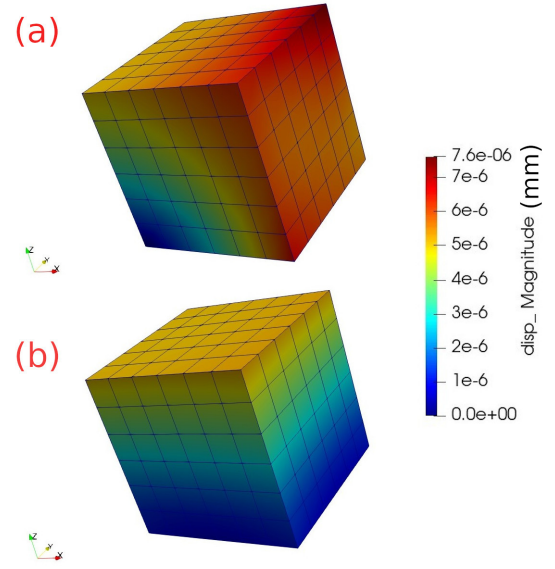


Fig. 5. Computed displacement at  $t=0.01$  s for deformation slip along  $\langle a \rangle$  direction for the (a) basal and (b) prismatic modes.

For the loading in the  $[001]$  direction, it is important to compare the magnitudes of effective Second Piola-Kirchoff stress between basal and pyramidal modes, and such comparison is provided in Fig. 7. As shown in the figure, when the strain along this direction is  $5.0\text{E-}5$ , the average magnitude of stress for Basal mode is 2.5 MPa whereas the effective stress for Pyramidal mode is above 4 MPa. These facts reveal

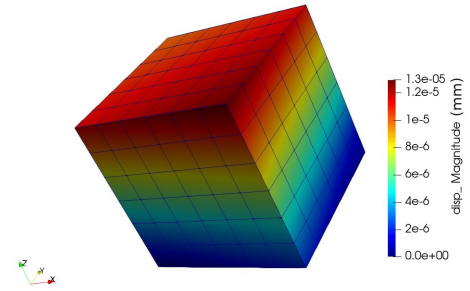


Fig. 6. Simulated displacement at  $t=0.01$  s for deformation along  $\langle c+a \rangle$  direction for the pyramidal deformation mode.

that the information obtained from crystal structure when used together with mesoscale simulations, can provide vast range of data about the materials behavior under external loading.

As illustrated by the magnitudes of stress above, it can be said that the current models are confined within the elastic regime. In context of applications of HCP  $\text{Cu}_6\text{Sn}_5$  IMC undergoing elasto-plastic loadings; these existing models have the capability to incorporate loadings that are large enough to induce stresses beyond the yield strength of the material.

In future, the numerical simulations will be performed in the plastic regime.

## V. CONCLUSIONS

The following conclusions have been derived from this study :

- 1) At temperature above 186 °C,  $\text{Cu}_6\text{Sn}_5$  IMC has a HCP structure. In this study, this structural information is utilized in the finite element method based deformation model at mesoscale.
- 2) The lattice constants and the elasticity tensors of  $\text{Cu}_6\text{Sn}_5$  IMC have been supplied to the mesoscale model as input materials parameters.
- 3) Three different modes of deformation - basal, prismatic and pyramidal, are considered in the mesoscale model. The displacement magnitudes in the three modes are studied for a given strain rate of  $5.0\text{E-}04 \text{ s}^{-1}$  in the Z-axis direction. It is found that the maximum displacement of the computational domain ( $\text{Cu}_6\text{Sn}_5$  IMC cube) under basal mode is larger as compared to that of prismatic mode. While all regions of the cube undergo a displacement in prismatic mode for the given loading condition, it is possible for some local regions in basal mode to not undergo deformation. In pyramidal deformation mode, all locations of the cube undergo displacement; and the magnitudes are larger compared to the other two modes.
- 4) For a given strain magnitude, the average value of Second Piola-Kirchoff stress in pyramidal deformation mode is larger as compared to the basal mode. This facts illustrate the importance of using atomistic informations in mesoscale simulations.

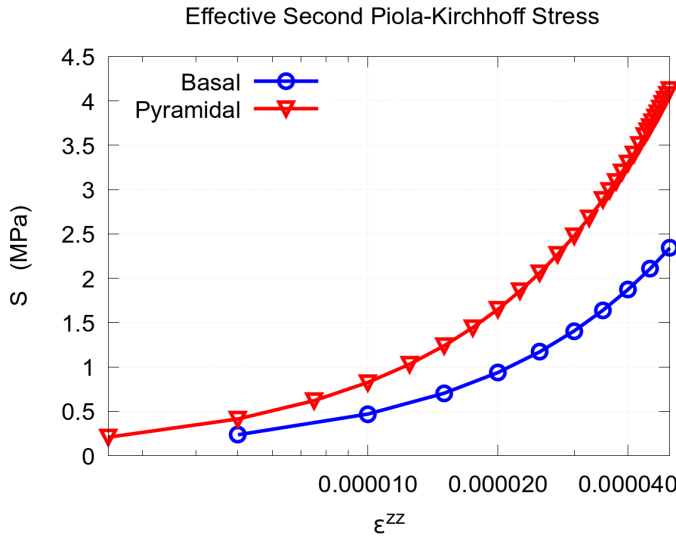


Fig. 7. Effective Second Piola-Kirchoff Stress versus strain along Z-direction for basal and pyramidal deformation modes.

## ACKNOWLEDGMENT

This work was supported by the National Science Centre, Poland (Grant Number: 2021/42/E/ST5/00339) and the National Natural Science Foundation of China (Grant Number: 52101035).

## REFERENCES

- [1] Chong Dong, Jinye Yao, Min Shang, Haoran Ma, Jun Chen, Haitao Ma, and Yunpeng Wang. New phenomenon: Cellular boundary during the isothermal stage in the Sn-3Ag/(0 0 1)Cu and Sn-3.5Ag/(0 0 1)Cu joint. *Materials Letters*, 317(March):132110, 2022.
- [2] Anil Kunwar, Johan Hektor, Sukeharu Nomoto, Yuri Amorim Coutinho, and Nele Moelans. Combining multi-phase field simulation with neural network analysis to unravel thermomigration accelerated growth behavior of  $\text{Cu}_6\text{Sn}_5$  IMC at cold side Cu-Sn interface. *International Journal of Mechanical Sciences*, 184(May):105843, 2020.
- [3] Xin F Tan, Shiwei Tao, Lingbing Ran, Ruth Knibbe, and Kazuhiro Nogita. Cobalt-doped Cu 6 Sn 5 lithium-ion battery anodes with enhanced electrochemical properties. *Nano Select*, (April):1–13, 2022.
- [4] D K Mu, S D McDonald, J Read, H Huang, and K Nogita. Critical properties of Cu 6 Sn 5 in electronic devices: Recent progress and a review. *Curr. Opin. Solid State Mater. Sci.*, 20(2):55–76, 2016.
- [5] Shuibao Liang, Anil Kunwar, Changqing Liu, Han Jiang, and Zhaoxia Zhou. Preferential growth of intermetallics under temperature gradient at Cu-Sn interface during transient liquid phase bonding: insights from phase field simulation. *Journal of Materials Research and Technology*, 19:345–353, 2022.
- [6] Johan Hektor, Matti Ristinmaa, Håkan Hallberg, Stephen A Hall, and Srinivasan Iyengar. Coupled diffusion-deformation multiphase field model for elastoplastic materials applied to the growth of  $\text{Cu}_6\text{Sn}_5$ . *Acta Materialia*, 108:98–109, apr 2016.
- [7] Chao Ding, Jian Wang, Tianhan Liu, Hongbo Qin, Daoguo Yang, and Guoqi Zhang. The Mechanical Properties and Elastic Anisotropy of  $\eta'$ - $\text{Cu}_6\text{Sn}_5$  and  $\text{Cu}_3\text{Sn}$  Intermetallic Compounds. *Crystals*, 11:1562, 2021.
- [8] Koichi Momma and Fujio Izumi. VESTA 3 for three-dimensional visualization of crystal, volumetric and morphology data. *Journal of Applied Crystallography*, 44(6):1272–1276, 2011.
- [9] N. T.S. Lee, V. B.C. Tan, and K. M. Lim. First-principles calculations of structural and mechanical properties of  $\text{Cu}_6\text{Sn}_5$ . *Applied Physics Letters*, 88(3):1–3, 2006.
- [10] M. Friák, D. Lago, N. Koutná, D. Holec, T. Rebok, and M. Šob. Multi-phase ELASTic Aggregates (MELASA) software tool for modeling anisotropic elastic properties of lamellar composites. *Computer Physics Communications*, 247:106863, 2020.
- [11] Romain Gaillac, Pluton Pullumbi, and François Xavier Coudert. ELATE: An open-source online application for analysis and visualization of elastic tensors. *Journal of Physics Condensed Matter*, 28(27), 2016.
- [12] Soud Farhan Choudhury and Leila Ladani. Single Crystal Plasticity Finite Element Analysis of  $\text{Cu}_6\text{Sn}_5$  Intermetallic. *Metallurgical and Materials Transactions A*, 46(3):1108–1118, mar 2015.
- [13] Cody J. Permann, Derek R. Gaston, David Andrš, Robert W. Carlsen, Fande Kong, Alexander D. Lindsay, Jason M. Miller, John W. Peterson, Andrew E. Slaughter, Roy H. Stogner, and Richard C. Martineau. MOOSE: Enabling massively parallel multiphysics simulation. *SoftwareX*, 11:100430, 2020.
- [14] Stephanie A. Pitts, Wen Jiang, Davide Pizzocri, Erin I. Barker, and Hussein M. Zbib. A Continuum Dislocation Dynamics Crystal Plasticity Approach to Irradiated Body-Centered Cubic  $\alpha$ -Iron. *Journal of Engineering Materials and Technology, Transactions of the ASME*, 144(1):1–9, 2022.
- [15] X. Deng, N. Chawla, K. K. Chawla, and M. Koopman. Deformation behavior of (Cu, Ag)-Sn intermetallics by nanoindentation. *Acta Materialia*, 52(14):4291–4303, 2004.